Wind and Structures, *Vol. 28, No. 1 (2019) 31-47*
DOI: https://doi.org/10.12989/was.2019.28.1.031

Wind tunnel tests and CFD simulations for snow redistribution on 3D stepped flat roofs

Zhixiang Yu*, Fu Zhu, Ruizhou Cao, Xiaoxiao Chen, Lei Zhao and Shichun Zhao

School of Civil Engineering, Southwest Jiaotong University, Chengdu 610031, China

(Received January 30, 2018, Revised December 26, 2018, Accepted December 29, 2018)

Abstract. The accurate prediction of snow distributions under the wind action on roofs plays an important role in designing structures in civil engineering in regions with heavy snowfall. Affected by some factors such as building shapes, sizes and layouts, the snow drifting on roofs shows more three-dimensional characteristics. Thus, the research on three-dimensional snow distribution is needed. Firstly, four groups of stepped flat roofs are designed, of which the width-height ratio is 3, 4, 5 and 6. Silica sand with average radius of 0.1 mm is used to model the snow particles and then the wind tunnel test of snow drifting on stepped flat roofs is carried out. 3D scanning is used to obtain the snow distribution after the test is finished and the mean mass transport rate is calculated. Next, the wind velocity and duration is determined for numerical simulations based on similarity criteria. The adaptive-mesh method based on radial basis function (RBF) interpolation is used to simulate the dynamic change of snow phase boundary on lower roofs and then a time-marching analysis of steady snow drifting is conducted. The overall trend of numerical results are generally consistent with the wind tunnel tests and field measurements, which validate the accuracy of the numerical simulation. The combination between the wind tunnel test and CFD simulation for three-dimensional typical roofs can provide certain reference to the prediction of the distribution of snow loads on typical roofs.

Keywords: wind tunnel test; adaptive-mesh method; numerical simulation; snow drifting; 3D stepped flat roof

1. Introduction

For structural engineers, it is important to accurately predict the snow distribution on roofs under the action of wind in regions with heavy snowfall. The snow distributions on roofs are always unevenly distributed due to snow drifting, which should be taken into account in the design of structures (Majowiecki 1998). Although there exists two-dimensional structures in nature, the snow drifting on typical roofs is affected by some factors such as building shapes, sizes and layouts to show more three-dimensional characteristics. Thus, research on three-dimensional snow distribution caused by snow drifting on roofs is needed. The techniques for prediction of snow drifting usually include field observation, wind or water tunnel tests and numerical simulations.

With the development of similarity criteria (Kind 1976, 1986, Iversen 1980, Kind and Murray 1982), Wind tunnel test is an effective method to reproduce snow drifting around buildings. Limited by the function of wind tunnels, the substitute for natural snow particles is always used in previous researches (Iversen 1980, Kind and Murray 1982, Anno 1985, Isyumov and Mikitiuk 1990, 1992, Schaelin *et al.* 2004, Zhou *et al*. 2014), and high-density silica sand is recommend to model the snow particle in recent years. Aside from the studies on snow drifting around buildings (Anno 1985, Kwok *et al.* 1992, Haehnel *et al*. 1993, Semdley *et al.* 1993), researchers have also studied snow redistribution on roofs. Isyumov and Mikitiuk (1990) carried out wind tunnel tests of snow drifting on the two-level roof under different wind velocity and focused on the mass transport rate and snow deposition pattern on the lower level roof. O'Rourke *et al.* (2004) studied snow patterns and snow mass transport rates on gable roofs, flat roofs and stepped flat roofs through water tunnel tests. Wang *et al*. (2014) studied the relationship of mass transport rate for three-dimensional stepped flat roofs with time in an open-circuit wind tunnel. Zhou *et al*. (2014) simulated snow drifting on two-dimensional stepped roofs with different spans using particles with different density. Zhou *et al.* (2016a) carried out simulation of snow drifting on flat roofs with different velocities and different span using silica sand and mass transport rate and mass flux were systematically studied.

Computational fluid dynamics (CFD) method has been rapidly developed since 1990s and some interesting studies have been presented in recent years. Uematsu *et al*. (1991) used CFD simulation to predict the snow drifting and did the pioneering work, which has been cited in most numerical simulations. Liston *et al*. (1993) conducted the numerical simulation of snow drifting around a two-dimensional snow fence. Thereafter, many researchers (Sato *et al*. 1993, Liston *et al*. 1994, Liston and Sturm 1998, Naaim *et al.* 1998) began to use and improve the numerical simulation method for snow drifting. Sundsbø (1998) employed one-way coupling model between the air and snow phase to simulate the wind deflection fins to control snow accumulation around a stepped building. Beyers *et al*. (2004) reproduced the transient snow drifting around a three-dimensional cubic model and the results showed there existed severe snow accumulation on the windward side of

*Corresponding author, Associate Professor
E-mail: yzxzrq@home.swjtu.edu.cn

ISSN: 1226-6116 (Print), 1598-6225 (Online)

the cube. Tominaga *et al.* (2006, 2009, 2011) presented a numerical simulation of three-dimensional snowdrift around a cubic building. Beyers and Waechter (2008) analyzed the transient snowdrift around complex three-dimensional structures. Zhao *et al.* (2016) simulated a two-dimensional snow drifting on the stepped flat roof using the combination of Eulerian and Lagrangian method. Zhou *et al.* (2016b) studied the snow drifting on a two-dimensional flat roof and the simulation results were in good agreement with the wind tunnel test. Zhu *et al.* (2017) conducted the numerical simulation of snow drifting on both two-dimensional and three-dimensional stepped flat roofs. Although numerical simulation method are more popular than the other two approaches in research, the validity of the numerical results still need to be verified using field observation or wind tunnel test (Liu *et al*. 2017).

Many studies aforementioned have been investigated snow distribution around buildings through the existing research methods. However, most of the studies have been only concerned about the mechanism of snow drifting or the effect of building shapes and layout on snow distribution around simple models. Only a few of them concerned about snow drifting on roofs, especially for two-dimensional roofs. Previous researches about the snow drifting on two-dimensional roofs have made some important achievements, but it is worth noting that real buildings have complicated geometric shapes and the snow drifting phenomena is complex. Due to the action of wind, the snow on three-dimensional roofs usually is affected by many factors to unevenly distribute. The parameters of roof type, span-height ratio, width-height ratio, and wind velocity, the incidence angle of the wind and snow properties will actually result in the change of characteristic of snow distribution, for example, the peak/valley position of snow and the position of deposition or erosion will change. Although the analysis of two-dimensional snow drifting can reveal some characteristic of snow distributions on the typical section, the three-dimensional analysis can provide certain reference to the prediction of the distribution of snow loads in both longitudinal and transverse directions. Tominaga (2017) summarized the research progress of snow drifting and also pointed out the prediction of roof snow loads is noteworthy in future research.

Field measurement is the most direct approach to obtain the snow distribution, however, this method has requirements on the environment of the test site and the factors such as weather conditions and thermal conditions of roofs, which will add uncertainties to the results of field measurements, are neither controllable nor repeatable. Therefore, the applicability of field data is limited for systematic and parametric studies. Generally, the field observations can only provide the pattern of snow accumulation as a qualitative validation for the other methods. In recent years, field measurements are rare and useable measurement data are rarely reported (Tutsumi *et al.* 2012). Compared with the field observations, the wind tunnel test of snow drifting can be carried out under controllable conditions. Based on the similarity law theory, the wind tunnel test is an effective and acceptable approach to reproduce the phenomenon of snow drifting on roofs, and the final snow distribution and mass transport rate are usually obtained due to the limitation of test equipment in wind tunnel test. The CFD technique can easily obtain the dynamic changes of flow field and snow cover boundary during the development of snow drifting, and provide some additional information. Wind tunnel tests are used in the literature (Naaim *et al.* 1998, Sekine *et al.* 1999, Okaze *et al*. 2015, Zhou *et al*. 2016b) as validations for numerical simulations. However, few studies in the previous literature have combined with numerical simulations with wind tunnel test to simulate the snow drifting (Zhou *et al*. 2016b).

This paper attempts to investigate the snow redistribution characteristics caused by wind action on stepped flat roofs under controllable conditions through the combination of wind tunnel tests and CFD simulations, where the final snow distribution and mass transport rate obtained from wind tunnel tests is used as validations for CFD simulations. Firstly, four groups of stepped flat roofs with width-height ratio w/H of 3, 4, 5 and 6 are designed, where w is the windward width of lower roof and H is the height of lower roof. Under the condition of a uniform approaching flow with a nominal wind velocity of 6.0 m/s, silica sand with the average radius of 0.1 mm is used to simulate the snow drifting on four stepped flat roofs in the wind tunnel. Three-dimensional snow distribution is obtained by 3D scanning when the test is finished. According to the reference (Zhu *et al.* 2017), adaptive-mesh method based on RBF interpolation is used to simulate the dynamic process of snow phase boundary on the stepped flat roof. Based on the similarity criteria, the wind velocity and wind duration are determined for CFD simulations. The commercial CFD software FLUENT 16.1 coupled with user C code is used in this study to model the transportation of snow particles. The duration of snow drifting will be divided into N stages and then a time-marching analysis of steady snow drifting on stepped flat roofs is carried out. The repose of angle of snow is taken into account in the initial stage, and the two-phase flow is regarded as a steady state in each stage (Zhou *et al.* 2016b, Zhu *et al*. 2017).The changes of friction velocity, snow cover boundary and mass transport rate can be obtained for each stage. Then, a comparison is made among snow distributions on lower roofs obtained from the CFD simulation, wind tunnel test and field observations (Tsuchiya *et al*. 2002) and the accuracy of the numerical simulation is validated. Finally, some effect of width-height ratio on snow drifting on lower roofs is analyzed.

2. Wind tunnel test

2.1 Similarity criteria

Snow drifting is a complex two-phase flow, and a number of similarity requirements must be satisfied between the model and prototype in a wind tunnel test. According to some related literature (Kind 1976, 1986, Iversen 1980, Zhou *et al*. 2014), the main similarity parameters include geometrical similarity, flow field similarity, particle motion similarity, deposit patterns

similarity and time similarity. According to Kind (1976, 1986), Iversen (1980) and Zhou *et al.* (2014), here a brief introduction of the main similarity parameters is given below, where subscript *m* and *p* represent the model and prototype.

To ensure the flow filed in a wind tunnel test is a fully rough flow and reduce the effect of viscosity, Eq. (1) should be satisfied and expressed as

$$\left(\frac{u_{*t}^3}{2gv}\right)_m \geq 30 \tag{1}$$

where u_{*t} is the threshold friction velocity, g is the acceleration of gravity, and v is the kinematic viscosity, which in the present study is taken as 1.45×10^{-5} m^2·s^{-2}. However, if the Eq. (1) is satisfied, the minimum value of u_{*t} is about 0.2 m/s. Dvorak (1969) and Kind (1976) pointed that the values of $u_{*t}^3/2gv$ would be below 30 and the effect of viscosity are still fairly small in this condition. Therefore, the Eq. (1) could be relaxed (Kind, 1976, 1986, Kind and Murray 1982).

Iversen (1979, 1980) held the view that correctly simulating of the aerodynamic roughness height under saltation conditions between the model and prototype was necessary, which can be expressed as below

$$\left(\frac{\rho u_*^2}{\rho_p Hg}\right)_m = \left(\frac{\rho u_*^2}{\rho_p Hg}\right)_p \tag{2}$$

where ρ_p is the particle density, ρ is the air density which is taken as 1.225 kg·m^{-3} in most studies, H is the characteristic height of models, u_* is the friction velocity.

Particle motion similarity includes the similarity of particle ejection process and trajectory between the model and prototype, which means the densimetric Froude number is the same. However, Iversen (1980) believed that the Froude number is not applicable in the wind tunnel test, and Anno (1984) pointed out that Froude number had a minimal influence on the final pattern of redistribution of snow. Thus, the densimetric Froude number could be relaxed. Kind (1976, 1986), Kind and Murray (1982) reported that a similar ejection process of particles must satisfy Eqs. (3) and (4)

$$\left(\frac{\rho_p}{\rho}\right)_m \geq 600 \tag{3}$$

$$\left(\frac{U(H)}{u_{*t}}\right)_m = \left(\frac{U(H)}{u_{*t}}\right)_p \tag{4}$$

where $U(H)$ is the velocity of approaching flow at the height of lower roof. Kind and Murray (1982), Kind (1986) and Zhou *et al*. (2014, 2016a) believed that a large density ratio results in relatively correct snow erosion/deposition patterns and transport rates in a wind tunnel test. Eq. (4) guarantees that the shear stress on snow surface is similar with respect to the threshold velocity of particles (Zhou *et al.* 2016b).

The following equation must be also satisfied to maintain the ratio of drag force to inertial force (Kind 1986), which can be expressed as

$$\left(\frac{w_f}{U(H)}\right)_m = \left(\frac{w_f}{U(H)}\right)_p \tag{5}$$

where w_f is the setting velocity of a particle.

A dimensionless parameter for duration ratio is defined based on the dimensionless volume of a leeward snowdrift between a model and its prototype (Anno 1984, Zhou *et al.* 2016b), which is expressed as

$$\left(\frac{tQ}{\rho_b H^2}\right)_m = \left(\frac{tQ}{\rho_b H^2}\right)_p \tag{6}$$

where t is the duration of snow drifting, Q is the mean mass transport rate which is calculated by the following equation

$$Q = \frac{\rho_b}{w\cdot t}\iint \Delta h(x,y)\,dxdy \tag{7}$$

where w is the width of windward side, $\Delta h(x,y)$ is the change of snow depth at the position (x, y) on roofs.

In addition, to obtain similar deposit shapes, a similar angle of repose is needed. However, this condition is difficult to achieve when modeling particles are used in wind tunnel test (Iversen 1980, Kind and Murray 1982, Anno 1984, Zhou *et al*. 2016a). The aforementioned similar parameters can be directly calculated by the determined scale ratio and particles property.

2.2 Particle selection and similar parameters

Kind *et al.* (1982) used low-density foam particles and high-density silica sand particles to simulate snow particles to carry out the wind tunnel test of snow distribution around the snow fences, respectively. The results showed that the snow distributions obtained by silica sand particles were in good agreement with the measured results than foam particles. Schaelin *et al*. (2004) used silica sand in water tunnel to carry out simulation of snow distribution around mountain cottage with scale ratio of 1/400, and the test results were in conformity with the measured data. Zhou *et al.* (2014) used the low-density saw wood ash, medium-density polyfoam, and high-density silica sand to simulate the snow distributions on stepped flat roofs in the wind tunnel. Zhou further verified that high-density silica sand could more accurately simulate the snow distribution on roofs. Thereafter, Wang *et al.* (2014) and Zhou *et al*. (2016a, b) also carried out the wind tunnel test of snow drifting on roofs using silica sand particles as snow particles.

Based on the previous research results, high-density silica sand has a better performance to reproduce the snow drifting phenomenon than low-density materials (Kind and Murray 1982, Zhou *et al.* 2014). Thus this paper uses the silica sand with the average radius of 0.1 mm in wind tunnel test, which is the same with the related literature (Kind and Murray 1982, Wang *et al*. 2014, Zhou *et al*. 2014, 2016a, b). In the beginning of the wind tunnel test, a thin layer of particles are uniformly paved on the baseboard. The wind velocity is increased until a number of particles begin to move, and then the wind velocity is decreased slowly. When

particles nearly cease to move, the wind velocity at the reference height is recorded. The friction velocity corresponding to this velocity is considered as the threshold friction velocity. However, due to the limitation of test instruments (cobra probe cannot be used in flow with fine particles), the threshold friction velocity measured by Wang *et al*. (2014) is used in this paper, and the value of u_{*t} is 0.15 m/s which is consistent with the value recorded in the literature (Kind and Murray 1982). The physical properties of silica sand are listed in Table 1.

Table 2 shows the values of the major similarity parameters of the CFD prototype and the scale model in wind tunnel test. There exist some differences between these values because the properties of snow particle are used in CFD simulations.

The Reynold number of aerodynamic roughness is 30.7 for CFD prototype and 11.9 for wind tunnel test. The value of 11.9 is close to the value of 13.0 recorded in the literature (Kind and Murray 1982). When the Reynold number of aerodynamic roughness is too small, it will lead to insufficient development of flow in the wind tunnel, which may affect the movement of particles. The similarity parameter of aerodynamic roughness height $\frac{\rho u_*^2}{\rho_p H_g}$ is in the same order of prototype, however, it is larger than the prototype. Zhou *et al.* (2016b) believed that the aerodynamic roughness height caused by particle saltation is not the major influence factor of flow field and the requirement of similarity parameter of $\frac{\rho u_*^2}{\rho_p H_g}$ could be relaxed. The densimetric Froude number of the wind tunnel test is different from the prototype, however, researchers (Anno 1984, Zhou *et al*. 2016b) pointed out that the similarity parameter of $\frac{\rho}{\rho_p-\rho}\frac{u_{*t}^2}{gd_p}$ and $\frac{\rho_p}{\rho_p-\rho}\frac{u^2(H)}{gH}$ could be relaxed. High-density silica sand is used in wind tunnel test, and the density ratio ρ_p/ρ is larger than 600, satisfying the requirement proposed by Kind and Murray (1982) and Kind (1986). However, using high density material will alter inertia forces on the model snow particles and makes them less susceptible to the effects of turbulence, which has not be evaluated in present analysis. The inlet condition of CFD and duration of wind are determined by Eqs. (4) and (6), respectively. Therefore, these two similarity parameters of velocity and time are the same between the model and the prototype. With reference to the similarity of particle trajectory, the ratio of settling velocity of silica sand and reference velocity is larger than that of prototype. However, the settling velocity of snow is between 0.2 m/s and 1.3 m/s (Satoh and Takahashi 2006, Zhou *et al*. 2016b) considering the inhomogeneity of snow particles. Thus, the value of $\frac{w_f}{U(H)}$ for prototype is in the range of 0.024 to 0.156. Thus, $\frac{w_f}{U(H)}$ of silica sand is within the range of the prototype.

Table 1 Physical properties of natural snow particle and silica sand

Properties	Snow particle	Silica sand
Diameter d_p (mm)	0.15	0.20
Particle density ρ_p ($kg \cdot m^{-3}$)	250	2560
Bulk density ρ_b ($kg \cdot m^{-3}$)	150	1670
Threshold friction velocity u_{*t} (m/s)	0.20	0.15
Setting velocity w_f (m/s)	0.20	0.60
Angle of repose θ (°)	50.0	34.5

Table 2 Similarity parameters of CFD prototype and tunnel test scale model

Similarity parameters	CFD (snow particle)	Wind tunnel test (silica sand)
$\frac{u_{*t}^3}{2g\nu}$	30.7	11.9
$\frac{\rho u_*^2}{\rho_p Hg}$	1.17E-05	5.06E-5
$\frac{\rho}{\rho_p-\rho}\frac{u_{*t}^2}{gd_p}$	0.141	0.017
$\frac{\rho_p}{\rho_p-\rho}\frac{U^2(H)}{gH}$	2.19	36.75
$\frac{\rho_p}{\rho}$	204.1	2089.8
$\frac{U(H)}{u_{*t}}$	41.6	41.6
$\frac{w_f}{U(H)}$	0.024	0.096
$\frac{tQ}{\rho_b H^2}$	0.156; 0.158; 0.160; 0.162	0.156; 0.158; 0.160; 0.162

2.3 Description of the test

The wind tunnel test is carried out in open-circuit wind tunnel called XNJD-2 at Southwest Jiaotong University. The test section is 10 m(x)×1.3 m(y)×1.5 m(z) and the stable wind velocity is from 0 to 19 m/s in test section. Fig. 1 illustrates the wind tunnel test layout of snow drifting for the stepped flat roof. Four groups of models which are made of PVC are included in this wind tunnel test, where the windward width w is 3*H*, 4*H*, 5*H* and 6*H*, respectively. The characteristic height *H* is 0.1 m (Fig. 1(b)).

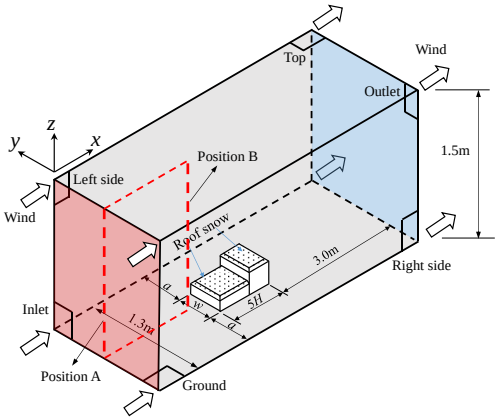

(a) layout of wind tunnel test

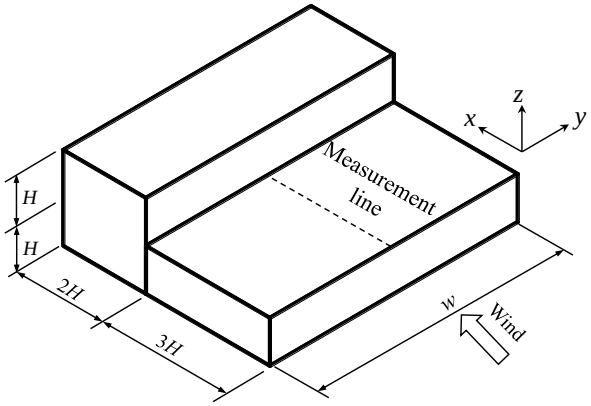

(b) stepped flat roofs model

Fig. 1 Diagram of wind tunnel test of stepped flat roofs

The geometrical scale ratio is 1:30. The blockage ranges from 3% for the model width of 3H to 6% for the model width of 6H. In order to avoid the outlet of wind tunnel influencing on the internal flow field, the distance between the model and the outlet is about 3.0 m.

In wind tunnel test, 20 mm silica sand particles are uniformly paved on stepped flat roofs to simulate the initial snowfall, where the lower roof is at windward side. A simple silica sand collecting device is placed at the outlet of the tunnel for reuse. The angle of the wind direction is 0° (Fig. 1(a)), without consideration of the change of wind direction.

Zhou *et al.* (2014) carried out wind tunnel tests of snow drifting on two-dimensional stepped flat roofs, in which the effects of wind duration on snow distribution were studied. Wang *et al.* (2014) carried out three-dimensional wind tunnel tests of snow drifting on typical roofs, and studied the relationship between mass flux and time. The determination of the wind duration in this paper is mainly referred to these existing literature.

The results of Zhou and Wang's research show that the choice of wind duration is related to the wind velocity. When the wind velocity is larger, a shorter wind duration is needed to form the stable snow cover. Under the condition of the same wind velocity, the length of wind duration will affect the depth of snow cover at the front region (windward side) on the centerline. When the wind duration is short, the coefficient of snow distribution is relatively large at the front region. For other regions, the coefficient of snow distribution at each time is relatively close. However, due to the strong separation around the three-dimensional model, the snow distribution in the roof edge region is significantly different in different time. The Fig. 2 shows the relationship of Mass flux over time obtained from the wind tunnel test. As can be seen from Fig. 2, the mass flux firstly increases with time, and then decreases with time when it reaches its maximum value, and finally tends to be stable as time increases. Considering that the wind tunnel equipment used in this paper is the same with the literature (Wang *et al.* 2014), and to reduce the test cost, the wind duration is chosen as 10 min. The wind duration 10 min for wind tunnel test corresponds to several hours for numerical simulation in Table 4. A real snow drifting phenomenon may last from hours to several days, thus 10 min duration is reasonable. When the wind duration is too short, the snow distribution has not fully developed. When the wind duration lasts too long, the erosion is serious, and more roof area is exposed.

The flow field needs to be measured in the test. The measuring positions are A and B in Fig. 1(a). The Position A is at the inlet of the wind tunnel and the position B is at the front of the model. Cobra probe is used to measure the wind velocity and turbulence intensity in wind tunnel. Because the cobra probe will be easily blocked and damaged by small particles, the measurement position is located at the front of models. When measuring, the cobra probe is fixed on the bracket, and the probe plane needs to be perpendicular to the flow direction. The cobra probe is connected to data collection box, and the sampling frequency and sampling time is 256 Hz and 60s, respectively.

Fig. 3(a) shows the distribution of the average wind velocity profile and the turbulence intensity at the nominal velocity of 6.0 m/s at the position A. The mean velocity profile is normalized by the wind velocity of the reference point at the height of lower roof $U(H)$. As one can see from Fig. 3a, the turbulence intensity at the height of H is about 5% and the approaching flow is close to the uniform flow. Wang *et al.* (2014) conducted a snow drifting test for typical

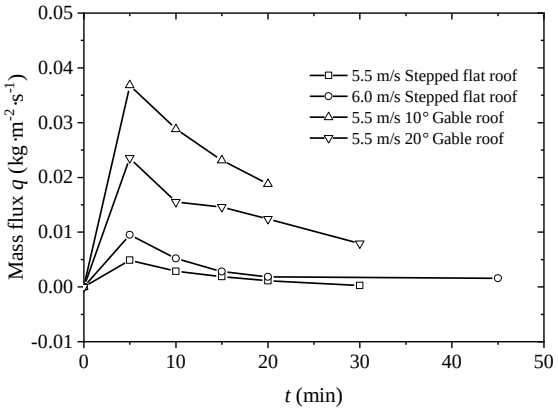

Fig. 2 The variation of Mass flux q with time (Wang *et al.* 2014)

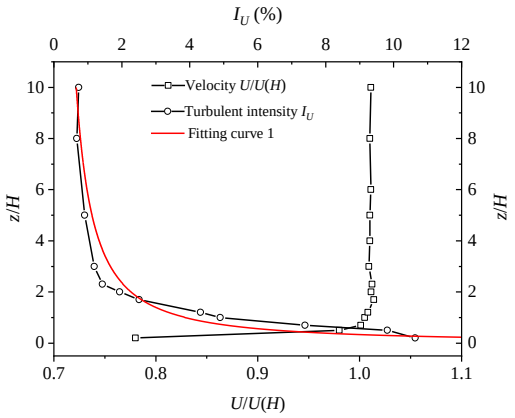

(a) Position A

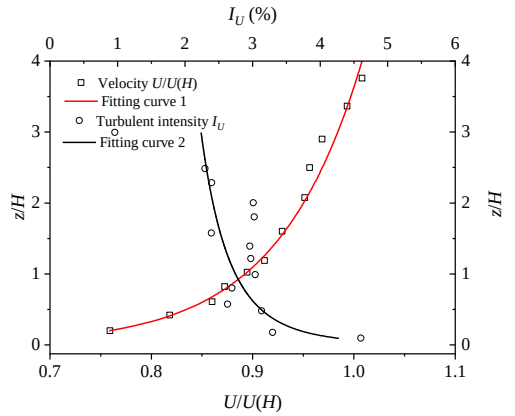

(b) Position B (Wang *et al.* 2014)

Fig. 3 Profiles of mean wind and turbulence intensity

roofs in XNJD-2 wind tunnel, and silica sand with the thickness of about 30 mm was uniformly paved on the surface of test section, of which length is about 3 m, to simulate the ground after snowfall. Wang measured the flow velocity through the silica sand bed and reported that the mean velocity was developed and well matched with the logarithmic law ($0 \le z/H \le 4.0$), and he measured the turbulence intensity below the relative position $0 \le z/H \le 4.0$ (Fig. 3(b)). At the relative height $0 \le z/H \le 2.0$, the mean wind velocity and turbulent intensity at position B are smaller than position A, showing the particles on the ground make the wind velocity and turbulent intensity decrease (Bintanja 2000, Wang *et al.* 2014).

2.4 Parameter definition

When a test case is finished, the snow depth on centerline (Fig. 1(b)) is measured by digital vernier caliper. Before using the digital vernier caliper, a zeroing operation is needed. Then, loosen the fastening screw and the depth bar is gently and perpendicularly inserted in the snow surface to the lower roof. And then, the length of depth bar is adjusted to slightly touch the snow surface. At the same time, the screw is tighten to fix the depth bar, and the numbers on the screen of digital vernier caliper are recorded.

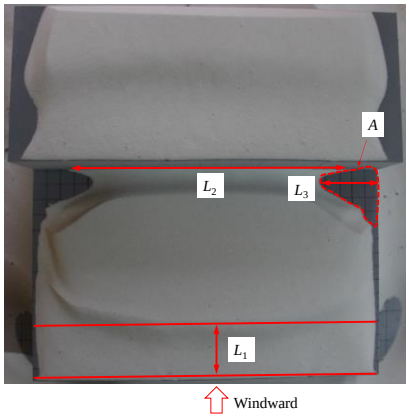

Fig. 4 Typical 3D snowdrift on the stepped flat roof in wind tunnel test

This number is the snow depth S at the measuring point. Meanwhile, 3D scanning is used to obtain the three-dimensional distribution of the snow depth on flat roofs. The normalized snow depth C_s is given by

$$C_S = \frac{S}{S_0} \tag{8}$$

where S is the snow depth on lower roof, for field observations S_0 is the snow depth on the ground, but for the numerical simulation and wind tunnel test, S_0 is the initial snow depth on the lower roof.

In order to describe the redistribution of snow on flat roofs due to the motion of creep, saltation and suspension caused by wind action (Fig. 4), η_i and λ are defined to describe the characteristic of 3D snow distribution, respectively.

$$\eta_i = \frac{L_i}{B_i} \times 100\% \tag{9}$$

$$\lambda = \frac{A}{wB_1} \times 100\% \tag{10}$$

where the subscript i is 1, 2 and 3, L_i is the length of the front erosion region, the length of the residual snow at the rear region and the length of bare roof, respectively, B_1 is the span of lower roof which equals to $3H$, B_2 and B_3 are both the width of the model which equal to w, A is the area of bare roof.

3. Numerical simulation

3.1 Dynamic control of snow phase

According to the overview literature of numerical simulation of snow drifting (Tominaga *et al.* 2011, Tominaga 2017), RANS equations of motion and Realizable k-ε model with standard wall functions are employed to model the turbulent air. These classical equations are not

given in this paper due to easily obtained in the other references. The equation that governs the snow phase (Uematsu *et al*. 1991, Tominaga *et al*. 2011, Zhou *et al*. 2016b, Zhu *et al*. 2017) as follows

$$\frac{\partial\left(\rho_s f\right)}{\partial t}+\frac{\partial\left(\rho_s f u_j\right)}{\partial x_j}=\frac{\partial}{\partial x_j}\left(\nu_t \frac{\partial \rho_s f}{\partial x_j}\right)+\frac{\partial}{\partial x_3}\left(-w_f \rho_s f\right) \quad (11)$$

where ρ_s is the density of snow, f is the snow volume fraction, $\rho_s f$ is the drifting snow concentration, u_j is the wind velocity calculated through the equations governing the air phase, ν_t is the turbulent kinematic viscosity, w_f is the vertical setting velocity of snow particles in still air. When steady state method is used in numerical simulations, the unsteady term on the left-hand in Eq. (11) will be set as zero. The additional convection term on the right-hand in Eq. (11) represents the convection effect by gravitational sedimentation. The erosive or accumulative snow fluxes on the snow surface as boundary conditions are calculated using the formula (Naaim *et al*. 1998, Beyers *et al*. 2004, Zhou *et al*. 2016b) as follows

$$q_{dep}=\phi w_f \frac{u_{*t}^2-u_*^2}{u_{*t}^2}, \qquad u_* < u_{*t} \quad (12)$$

$$q_{ero}=-A\rho\left(u_*^2-u_{*t}^2\right), \quad u_* > u_{*t} \quad (13)$$

$$u_*=\sqrt{\tau_* / \rho} \quad (14)$$

where ϕ is the snow concentration equal to $\rho_s f$, A is a proportionality coefficient representing the bonding strength of snowpack, usually $A\rho=7\times10^{-4}$ is employed (Naaim *et al*. 1998, Beyers *et al*. 2004, Zhou *et al*. 2016b, Zhu *et al*. 2017), ρ is the density of air, τ_* is the flow shear stress on the snow surface which can be obtained from the numerical results of air field. Thus, the total mass flux q_{total} on the snow surface is given by

$$q_{total}=q_{ero}+q_{dep} \quad (15)$$

Therefore, the change of snow depth is given by

$$\Delta h=\frac{q_{total}}{\rho_s}\times\Delta t \quad (16)$$

where Δt is the possible physical time interval for a snow drifting.

The commercial CFD software FLUENT is employed in this paper, which stores flow field data in the cell and face and space coordinates in the node. According to the reference (Zhou *et al*. 2016b), a simple two-dimensional mesh adjustment method is shown in Fig. 5, where the subscript F represents the face centroid and subscript i represents the face centroid numbering. When the number of nodes is large, the boundary of snow surface would be smooth enough. Applying this method to a three-dimensional model, however, the point set $\{(x_F, y_F, _{new})_i\}$ in plane will be expanded to point cloud $\{(x_F, y_F, z_F, _{new})_i\}$ in space. It is complex to reconstruct surface using point cloud and there may exist a continuity problem between the reconstruction surface and the initial model (Zhu *et al*. 2017).

For the issues mentioned above, an adaptive mesh method based on the radial basis function (RBF) interpolation proposed by Zhu *et al*. (2017) is used to simulate the dynamic change of snow phase boundary on lower roofs in this study. Here is a brief introduction. Two steps are included in this method: firstly RBF interpolation is used to adapt the boundary and then a mesh law is introduced to adjust the mesh. A typical multi-input and single-output RBF topological structure includes the input, basis function and output. Because of a good precision to approximate a smooth mapping of input-output (Powell 1987), Multiquadric function is used as the basis function in this paper. The schematic diagram of boundary adaption based on RBF interpolation is shown in Fig. 6, where the subscript j and N represent the node numbering and the node, respectively.

Finally, a mesh law is introduced to solve the mesh quality problems after boundary adaption (Fig. 7). The mesh law Geometric1 is used, which can be expressed as

$$S_i=\frac{R-1}{R^N-1}\sum_{j=2}^{i}R^{j-2} \quad (17)$$

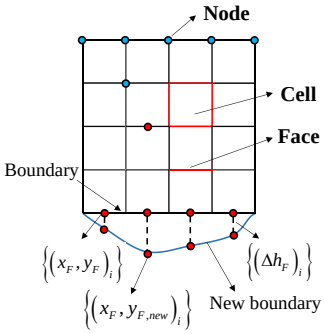

(a) Data structure

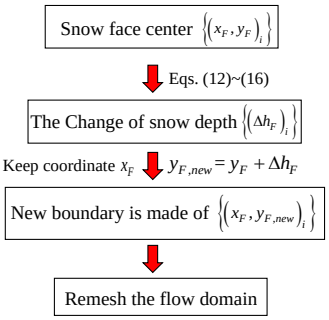

(b) Adjustment process

Fig. 5 Adjustment method of 2D mesh

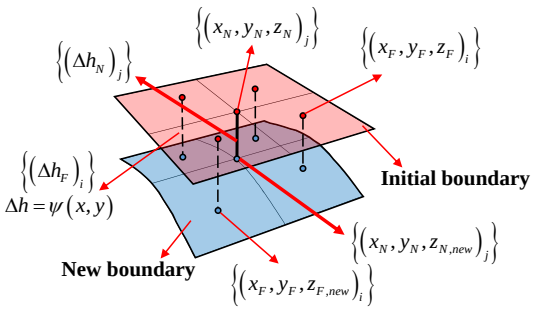

Fig. 6 Method for boundary adaption based on RBF interpolation (Zhu *et al.* 2017)

where S_i is the distance from the start of edge to the node i, R is the rate which is in the range of 0.25 to 4, N is the total node number. When using the mesh law Geometric1, the distance S_1 and N should be specified firstly and then the nodes are generated on the edge of unit length (the length is 1). Finally all the nodes are mapped to the actual edge. When the minimum grid size is specified as d, S_1 is a determined value of d/L_i, where L_i is the length of edge i in a certain stage of the mesh adjustment. When adjusting the mesh, repeat the above process and then all nodes are mapped to the new edge. Therefore, the minimum grid size of snow surface can be precisely controlled as a specified value in the subsequent mesh adjustments. The detailed governing equations for this method can be found in the reference (Zhu *et al*. 2017).

3.2 Time-marching method for stepped flat roofs

The time-marching method or quasi-steady method based on steady-state algorithm for the simulation of snow drifting has been developed recently and this method can solve the problems of high time-consuming and the correspondence between computational time and the real time. This paper extends the steady calculation method which was proposed in references (Zhou *et al.* 2016b, Zhu *et al.* 2017) and develops it with RBF adaptive mesh method for the snow drifting on stepped flat roofs. The duration T is determined based on wind tunnel test data and then divided into N stages. In each stage, the snow drifting is regarded as a steady state and the one-way coupling and adaptive mesh method aforementioned in Sections 3.1 is used to calculate the snow drifting on roofs. Wind tunnel test (Wang *et al.* 2014) and numerical simulation (Zhu *et al.* 2017) results show that the mean mass transport rate of snow on roofs tends to be stable over time, so the mean mass transport rate and its residual are used as the basis for judging whether the calculation is convergent or not. According to the reference (Zhu *et al.* 2017), the optimum iteration method is used to determine the optimal value of N to balance the computational accuracy and efficiency. The relative residual ζ of the mean mass transport rate of snow phase is defined as follows

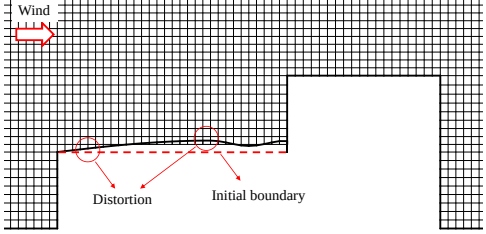

(a) Distortion

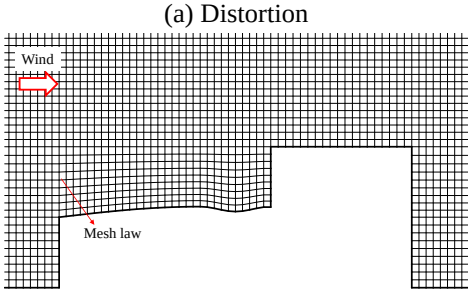

(b) Mesh adjustment

Fig. 7 Mesh adaptation

$$\xi = \left| \frac{Q_{m,i+1} - Q_{m,i}}{Q_{m,i+1}} \right| \le \xi_0 \tag{18}$$

where the subscript i represents the ith calculation, $Q_{m/+1}$and $Q_{m,i}$ are the mean mass transport rate of the (i+1)th calculation and ith calculation, respectively, and ζ_0 is the relative tolerance which is a small constant equal to 0.05. The ith calculation is corresponding to N_i. When $\zeta \le \zeta_0$ is met, iterative convergence is reached and N_{i+1} is the optimal value. The specific processes are as follows:

(1) Base on wind tunnel test data, the duration T is determined and divided into N_i stages (i=1, 2, 3⋯). Initialize $N_i = n$, where usually N_1=2.

(2) The steady flow field is obtained by solving RANS equations. Friction velocity u_* of stage k on snow surface can be calculated with the steady flow field, where k is a certain stage in the range of 1 to N.

(3) The governing equation of snow phase (Eq. (1)) is solved according to flow field characteristics. And then the change of snow depth Δh_k can be calculated based on Eqs. (12) to (16). The snow depth of stage k+1 is calculated by the following equation

$$h_{k+1} = h_k + \Delta h_k + d_k \tag{19}$$

where h_k and h_{k+1} are initial snow depth of stage k and stage k+1, respectively, and d_k represents the snow depth as a result of snowfall, sublimation and repose angle and so on.

(4) Adaptive mesh program using RBF interpolation is applied to adjust snow boundaries at the end of stage k and generates a new mesh for stage k+1. Steps 2-4 are repeated until the final stage n. The average mass transport rate of stage N_i is calculated.

(5) Set n=n+1 and i=i+1. Repeat steps 1-4. If the condition $\zeta \le \zeta_0$ is met, the iteration is convergent. Finally, n+1 is taken into account as the most rational value of N.

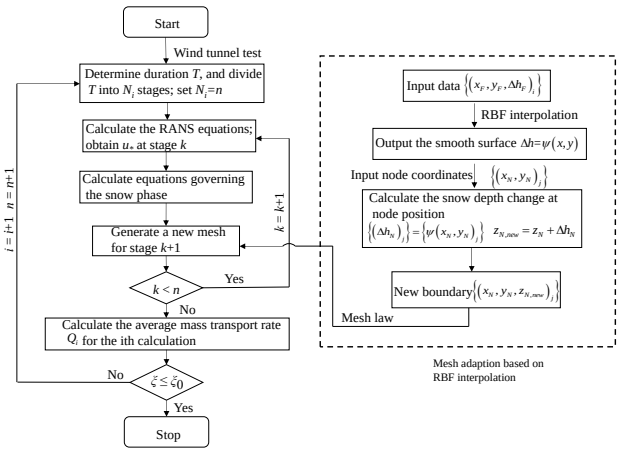

Fig. 8 Flow chart of calculation

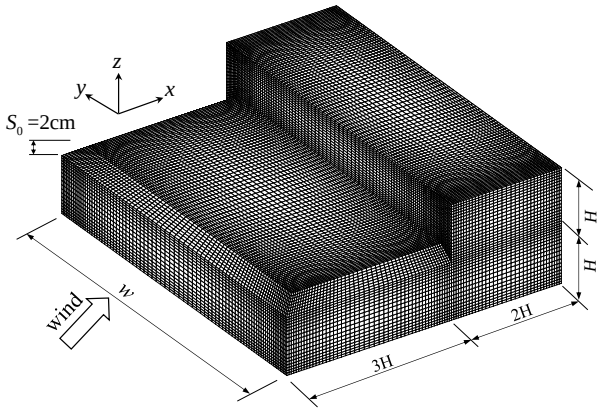

Fig. 9 Diagram of calculation model

Fig. 8 shows the calculation processes of snow drifting based on the time-marching method using RBF interpolation. Therefore, this method can take into account the effects of snow boundary changes in stage k on stage k+1 and then predict the phase boundary changes between the air and snow over time.

3.3 Numerical simulation parameters

Corresponding to wind tunnel test, the windward width of the model w is 3H, 4H, 5H and 6H for numerical simulation, respectively, where the characteristic height H is 0.1m as well. The results of numerical simulations (Wang *et al*. 2013, Zhao *et al*. 2016, Zhu *et al*. 2017) and wind tunnel tests (Zhou *et al*. 2014, Wang *et al.* 2014) with different H show that the dimensionless snow depth is good consistent with the field observations (Tsuchiya *et al*. 2002) in centerline. Although the sizes of stepped flat roofs are different, the dimensionless snow depth is similar to each other under the condition that the wind velocity and direction is kept the same in wind tunnel tests and numerical simulations. Therefore, in order to combine with the wind tunnel test aforementioned, characteristic length H=0.1m is adopted in the numerical simulation.

According to the references (Kuroiwa *et al.*,1967, Zhou *et al*. 2016b), this paper supposes that the temperature is below 0 ℃ during snow drifting and repose angle of snow is 50°. The partial calculation model considering the angle of repose is shown in Fig. 9, of which the initial snow depth is 0.02m on the lower roof. According to some related literature (Beyers *et al.* 2004, Franke *et al.* 2007, Tominaga *et al*. 2008, Blocken 2015), the computational domain is 90 H(x)×13 H(y)×15 H(z) and the distance from the stepped flat roof to the inlet boundary is 30H. Structured progressive mesh is used as mesh scheme for four models. According to the references (Tominaga *et al*. 2015, Zhou *et al.* 2016), the prediction results did not change significantly with finer grids, so the minimum grid size near the snow surface is set as H/30. The total number of grid cells in the three-dimensional model is about 2.5 million. For the convection terms of the equations, the second order scheme is used.

Corresponding to the wind tunnel test, the inlet velocity profile is described by a uniform flow and expressed as

$$u(z)=U(H) \tag{20}$$

where $u(z)$ is the wind velocity at the height of z (m). Realizable $k-\varepsilon$ model is employed to describe the turbulent flow in this paper, and turbulent intensity and viscosity ratio is used to determine the inlet profile of turbulent kinetic energy and turbulent dissipation rate.

$$k=\frac{3}{2}(u_{\text{avg}}I)^2 \tag{21}$$

$$\varepsilon=\rho C_\mu \frac{k^2}{\mu}\left(\frac{\mu_t}{\mu}\right)^{-1} \tag{22}$$

where u_{avg} is the mean flow velocity, I is the turbulent intensity, C_μ is an empirical constant specified in the turbulence model and C_μ=0.09, μ is the air viscosity, $\frac{u_t}{u}$ is the turbulent viscosity ratio. According to FLUENT User's Guide, the turbulent intensity and viscosity ratio is specified as 5% and 10, respectively. To reduce the effect of blockage, symmetry boundary is used in CFD simulations.

The boundary condition of snow phase is also needed. In this paper, it is assumed that there is no snowfall when snow drifting occurs and the initial snowpack on the lower roof is taken into consideration. According to some related literature (Beyers *et al*. 2004, Franke *et al*. 2007, Tominaga *et al.* 2008, Zhao *et al*. 2016, Zhou *et al.* 2016b), the boundary conditions for air and snow phase are summarized in Table 3, in which ψ denotes all flow variables except pressure.

Table 4 presents the major parameters of numerical simulation. The inflow velocity, the threshold friction velocity of silica sand particles in wind tunnel test is known, and the threshold friction velocity of snow particles in numerical simulations is also given. So the inflow velocity in numerical simulations can be calculated by Eq. (4). Only when the threshold friction velocities of silica sand particles

and snow particles are the same, the inlet velocity in numerical simulation will be equal to the wind tunnel test. So $U(H)$, the velocity of uniform flow in the inlet boundary, is 8.32 m/s determined by Eq. (4). When the wind velocity is different, the mean mass transport rate of particles is also different. In order to ensure the similarity of snow distribution between the wind tunnel test and numerical simulation, the wind duration of the numerical simulation is controlled by Eq. (6). It can be seen from Eq. (6) that because the density and mean mass transport rate for both of silica sand particles and snow particles are different, the wind duration in the numerical simulation is also different from that in the wind tunnel test. The wind duration of each model in CFD simulations is calculated by the results from wind tunnel test. When the wind duration of the model in the wind tunnel test is fixed, the numerical simulated mean mass transport and experimental results can be obtained by Eq. (7). Therefore, the wind duration of numerical simulations could be calculated by Eq. (6). Given that a snowstorm may last from hours to several days, the wind duration of numerical simulation is set as 4.0 hours, 5.1 hours, 6.7 hours and 8.2 hours for four models, respectively. According to time allocation method used in the reference (Zhu *et al*. 2017), the time interval of the first stage in this paper is set as 1.0 hour, and the remaining hours are uniformly divided into N-1 parts.

Table 3 Boundary conditions for numerical simulation of wind-driven snow

Model boundary name	Type	Air phase	Snow phase
Inlet	Velocity-inlet	$u_z = \text{Eq.}(20)$ $k = \text{Eq.}(21)$ $\varepsilon = \text{Eq.}(22)$	$f = 0$
Outlet	Outflow	$\partial\Psi / \partial n = 0$	$\partial f / \partial n = 0$
Building walls	Wall（Standard wall function）	$u, v, w = 0$	$f = 0$
Snow surface			$q = \text{Eqs.}[(12) \sim (13)]$
Ground			$f = 0$
Top face and sides	Symmetry	$\partial u / \partial n = 0$	$\partial f / \partial n = 0$

Table 4 Parameters of the numerical simulation

Parameters		CFD	Wind tunnel test
Geometric scale ratio		1:30	1:30
Initial snow depth (mm)		20	20
Wind velocity at lower roof height in the inlet boundary (m/s)		8.32	6.24
Turbulence intensity at lower roof height in the inlet boundary (%)		5.0	5.0
Wind duration	w/H=3.0	4.0h	10min
	w/H=4.0	5.1h	
	w/H=5.0	6.7h	
	w/H=6.0	8.2h	

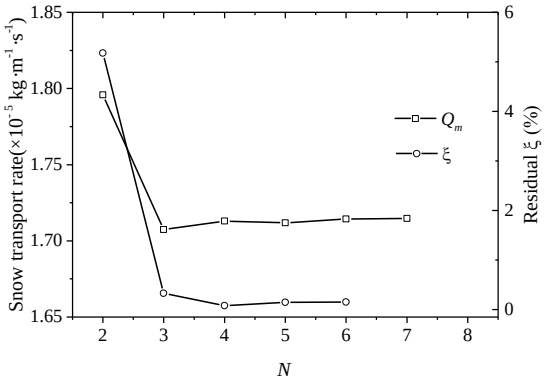

(a) w/H=3.0

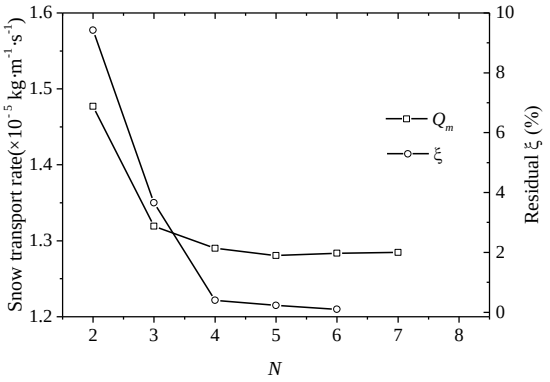

(b) w/H=4.0

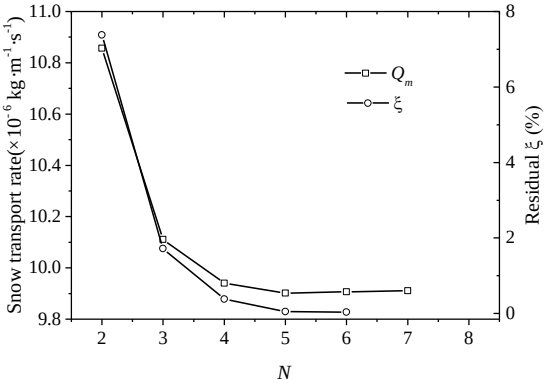

(c) w/H=5.0

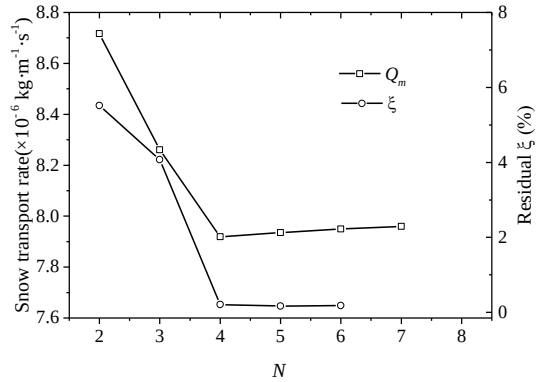

(d) w/H=6.0

Fig. 10 Determination for the optimal value of N

Fig. 10 gives the effect of N on the average mass transport rate Q_m and the relative residual ζ. As one can see from Fig. 10, Q_m and ζ tend to be stable with the increase of N. When N=4, the relative residual ζ of four models satisfies the Eq. (18). Therefore, the duration T for the calculation of snow drifting on stepped flat roofs is divided into four stages, which is the same with the reference (Zhu *et al*. 2017).

Four stages are represented by 1, 2, 3 and 4. The subscript S (Start) represents the initial time of a certain stage and the subscript E (End) represents the end of a certain stage in the following sections.

4. Results

4.1 Results of wind tunnel test and numerical simulation

Fig. 11 presents the photographs of the snow distribution on the lower roofs at the end of the wind tunnel test. In general, three regional distribution of snowpack on lower roofs is obvious (Fig. 11(a)). There exists a distinct arc-shaped interface region 1 and region 2, while the exposed roof, caused by severe erosion, at left and right corners at region 3 are basically symmetrical. The normalized distribution of snow depth on lower roofs for the wind tunnel test and numerical simulation are shown in Figs. 12-15. It can be seen that the snow on the lower roof of four models mainly present as erosion and the erosion of snow concentrates on the edge and corner of the lower roofs. The deposition mainly occurs in the middle region due to the relatively low friction velocity (Fig. 17), while the deposition amount is low and the region of deposition is small.

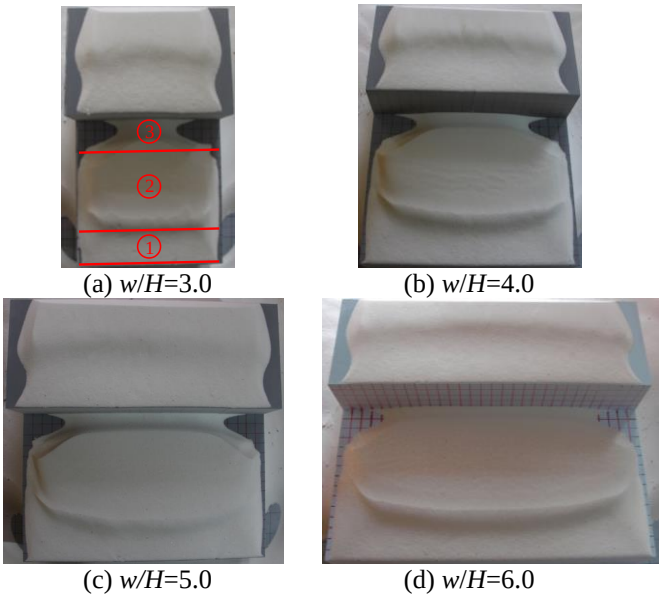

(a) w/H=3.0 (b) w/H=4.0

(c) w/H=5.0 (d) w/H=6.0

Fig. 11 Photograph of four models in wind tunnel test

However, the deposition amount of wind tunnel test is larger than that in numerical simulation, and the position where deposition occurs is closer to the rear region of the lower roof. The maximum normalized snow depth is about 1.1 for wind tunnel tests. As one can see from the figures, the snow depth distribution presents hill-shaped.

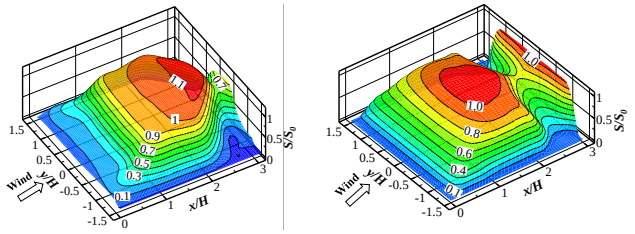

(a) wind tunnel test (b) CFD simulation

Fig. 12 Snow depth distribution on the lower roof for w/H=3.0

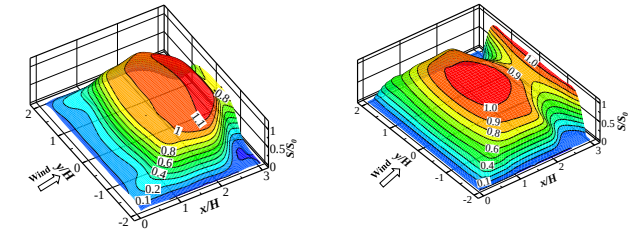

(a) wind tunnel test (b) CFD simulation

Fig. 13 Snow depth distribution on the lower roof for w/H=4.0

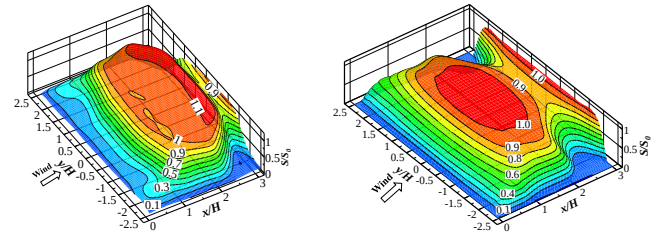

(a) wind tunnel test (b) CFD simulation

Fig. 14 Snow depth distribution on the lower roof for w/H=5.0

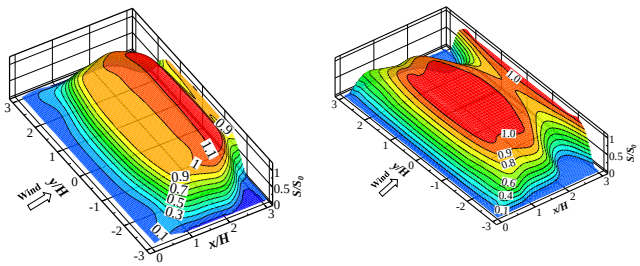

(a) wind tunnel test (b) CFD simulation

Fig. 15 Snow depth distribution on the lower roof for w/H=6.0

For the models with the same width-height ratio, the snow depth of the rear region (near x/H=3.0) in wind tunnel tests is smaller than that in numerical simulations. The snow surface will be steep with the development of erosion and the snow particles on the surface layers will be slipping along the steep surface due to the effect of angle of repose. Thus, the snow depth of this region will decrease. However, the effect of angle of repose in the process of snow drifting is not yet considered in the numerical simulation for the present study, which is probably the main reason for the differences between the numerical simulation and the wind tunnel test at the rear region. In addition, the limitation of k-ε model may be another reason. It is well known that the turbulent kinetic energy may be underestimated at the rear region of the lower roof (Murakami 1993, Murakami e*t al*. 2003), which will also cause the erosion of numerical simulation at the rear region less than that in the wind tunnel test.

With the increase of the width-height ratio w/H, the relative area of exposed roofs at the rear region decreases, so that the distribution of snow depth on lower roofs looks like more uniform in the transverse direction. When the width-height ratio w/H gradually increases, the percentage of snow erosion on lower roofs in wind tunnel tests is 31.29%, 30.14%, 29.29% and 28.83%, respectively, while it is 31.86% 29.27%, 29.68% and 28.65%, respectively, in numerical simulations. The results between wind tunnel tests and numerical simulations are basically consistent.

4.2 Comparison of numerical simulation results with the test and measured data

Fig. 16(a) shows the normalized snow depth distribution of lower roof at the centerline (y/H=0) from both the numerical simulation and the wind tunnel test. As plotted in Fig. 16, three regions including the front region ($0<x/H<0.75$), the middle region ($0.75<x/H<2.25$) and the rear region ($2.25<x/H<3.0$) are classified to describe the change of the redistribution of snow and friction velocity, according to the change feature of friction velocity and dimensionless snow depth. The results of the wind tunnel test are first analyzed. The erosion and deposition status on the lower roof are reflected in Fig. 16(a). The particles at the front region of fours models are severely eroded during the wind tunnel test. A few particles deposited at the middle region and the normalized snow depth gradually increases with the relative position x/H. Then, the maximum of snow depth appears and the relative position x/H is about 2.6. As one can see from Fig. 16a, the snow depth of four models in the wind tunnel test coincides each other at the relative position $1.0<x/H<2.5$. The erosion is extreme non-uniform due to the vortex at the rear region. The results of the numerical simulation are then analyzed. The overall trend of the numerical simulation is consistent with the wind tunnel test. However, the relative position of the maximum snow depth is of some differences with the wind tunnel test. The relative position of the maximum snow depth for the numerical simulation is in the range of 0.75 to 1.25, where the upper limit is for the width-height ratio w/H=6.0 and the lower limit is for the width-height ratio w/H=3.0.

Compared the results obtained from the numerical simulation with the wind tunnel test, some consistent points as well as differences can be concluded. With the increase of width-height ratio w/H, the snow erosion decreases at the front and rear regions for both the numerical simulation and wind tunnel test. The snow depth of numerical simulation at the relative position $1.0<x/H<2.5$ is in good agreement with the wind tunnel test.

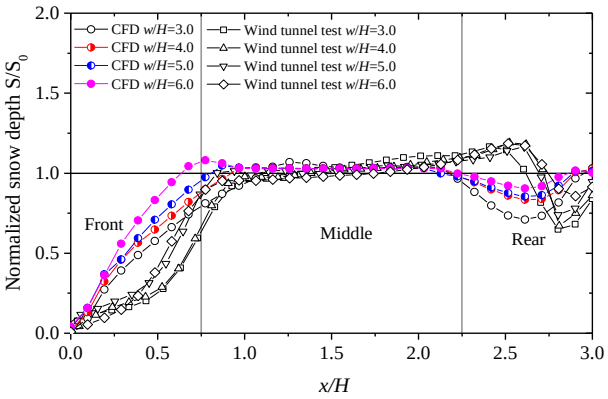

(a) CFD and wind tunnel test

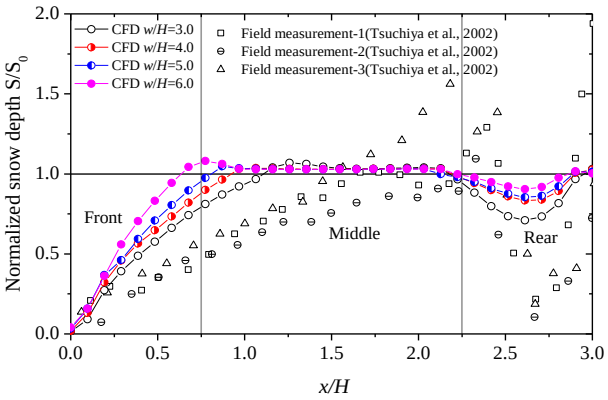

(b) CFD and field observations (Tsuchiya *et al*. 2002)

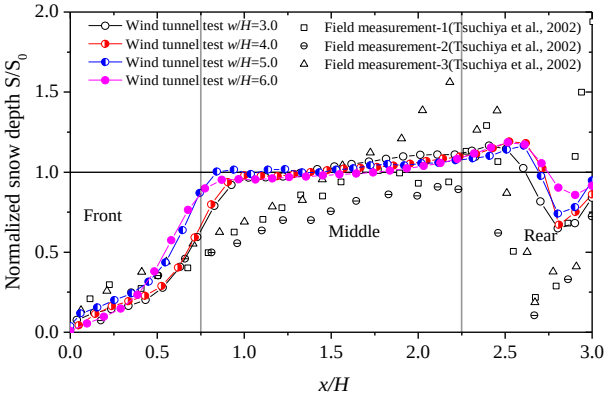

(c) Wind tunnel test and field observations (Tsuchiya *et al.* 2002)

Fig. 16 Snow depth distribution on the lower roof at y/H=0

However, the dimensionless snow depth of numerical simulation is larger than the wind tunnel test at the front region of lower roofs ($0<x/H<0.75$). The main reason is probably that the normal component of the erosion caused by impinging flow is not considered in numerical simulation and actually it exists in wind tunnel test (Humphrey 1990, Beyers *et al*. 2004). At the rear region of the lower roof, numerical simulation also predicts the non-uniform erosion which is slightly smaller than the wind tunnel test. The erosion position of numerical simulation is closer to the windward side than the wind tunnel test and the center of erosion position is about 2.6 and 2.8 for the numerical simulation and wind tunnel test, respectively. Meanwhile, there exists an obvious snow accumulation in the front of the erosion pit for the wind tunnel test, which is not observed in the numerical simulation.

Fig. 16(b) presents the comparison between the results of the numerical simulation with field observations carried by Tsuchiya *et al*. (2002) with w/H=6.0, while Fig. 16(c) shows the comparison between the results of wind tunnel tests with field observations with w/H=6.0 (Tsuchiya et al., 2002). For the same width-height ratio w/H=6.0, the snow depth at the relative position $0.5<x/H<1.5$ for the numerical simulation and at $0.75<x/H<1.5$ for the wind tunnel test is higher than three field measurements, while erosion quantity at the rear region of both the numerical simulation and the wind tunnel test is lower than field observations. These differences may be caused by differences of wind velocity, wind directions, measurement time, the location for the model and the properties of snow particles. Although there exist some differences, the overall trend of the numerical simulation and the wind tunnel test results are consistent with field observations in general.

5. Analysis and discussion

5.1 The influence of width height ratio on friction velocity u_*

Fig. 17 shows the influence of width-height ratio w/H on the friction velocity u_* of centerline (y/H=0) on the lower roof. The vertical axis denotes the dimensionless friction velocity, which is the ratio of friction velocity u_* at the start of each stage on the lower roof to the threshold friction velocity u_{*t}. In general, the distributions of friction velocity for four models, which is simulated numerically, resemble each other for a certain stage. It can be seen that the width-height ratio has some impact on the distribution of friction velocity from Stage 1_S to Stage 4_S. At Stage 1_S, the friction velocity of four models at the front region is larger than the threshold friction velocity due to the strong separation and the friction velocity of w/H=3.0 is slightly higher than the others. It is noteworthy that the friction velocity distributions of w/H=4.0 to 6.0 basically coincide at the front and middle region at Stage 1_S, and the valley points at the middle region for these three models are close to the relative position x/H=0.90. However, the distribution of friction velocity distributions for w/H=3.0 has a relatively large difference with the others at middle region, and the valley point is about x/H=1.55. The peak values at the rear region gradually decrease with the increase of width-height ratio.

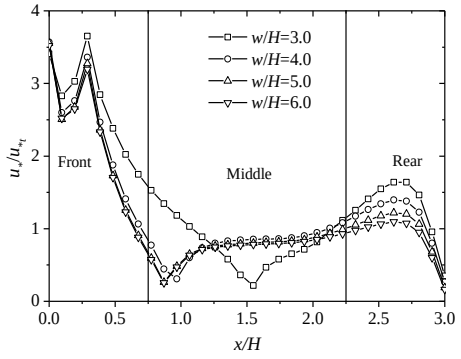

(a) Stage 1_S

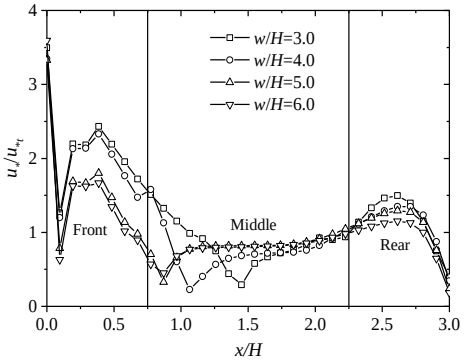

(b) Stage 2_S

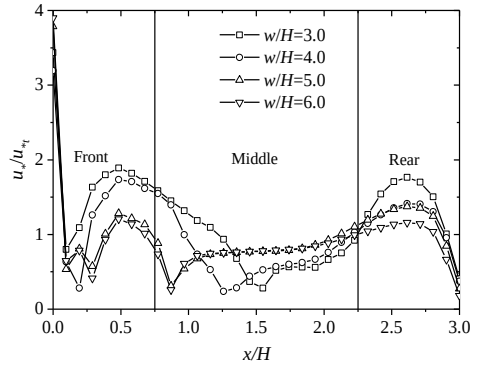

(c) Stage 3_S

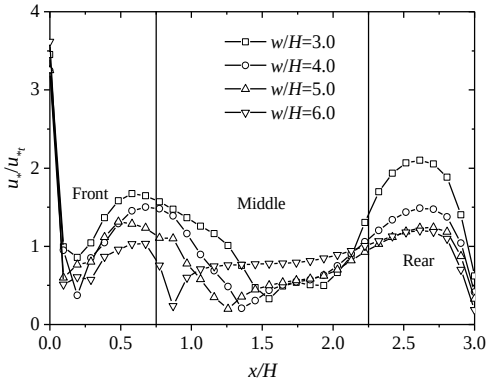

(d) Stage 4S

Fig. 17 Distribution of friction velocity on the lower roof at y/H=0

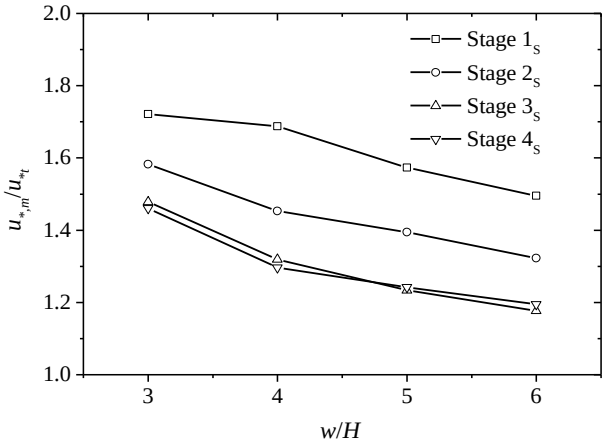

Fig. 18 Variation of the mean friction velocity u_{*m} with w/H

Significant erosion of snow at the front region occurs due to the large friction velocity, and this change of snow cover profile also alters the flow field around the front region. This condition explains why the friction velocity at the front region changes drastically for Stage 2_S to 4_S. At Stage 4_S, the distribution of friction velocity on centerline is more obviously related to width-height ratio. The friction velocity at the front and rear region decreases with the increase of width-height ratio. In the middle region of Stage 4_S, the relative position x/H of valley points are 1.55, 1.35, 1.16 and 0.87, respectively, with the increase of the width-height ratio. Compared with the first stage, the relative position x/H of valley points for w/H=3.0 and w/H=6.0 are basically the same, while it is closer to the rear region for w/H=4.0 and w/H=5.0. Therefore, it can be found that the effect of width-height ratio on the distribution of friction velocity on the centerline (y/H=0) is significant at the start of the last stage, especially w/H is 4.0 and 5.0.

To further analyze the influence of the width-height ratio on the friction velocity, Fig. 18 illustrates the relationship between the mean friction velocity u_{*m} on the lower roof and the width-height ratio w/H. Dimensionless friction velocity is the ratio of the mean friction velocity u_{*m} to the threshold friction velocity u_{*t}. The mean friction velocity decreases with the increase of width-height ratio for all of the stages, which can explains that the snow erosion amount is large with relatively small width-height ratio to some extent. With the development of snow drifting, the mean friction velocity decreases gradually and are basically in coincidence at Stage 3_S and Stage 4_S, which means the snow mass transport rate would be stable.

5.2 The characteristic of snow distribution on lower roofs

Fig. 19 presents the variation of the characteristic of snow distribution on the lower roof with the width-height ratio. The dimensionless length η_1 of the erosion at the front region decreases as the width-height ratio (Fig. 19(a)).

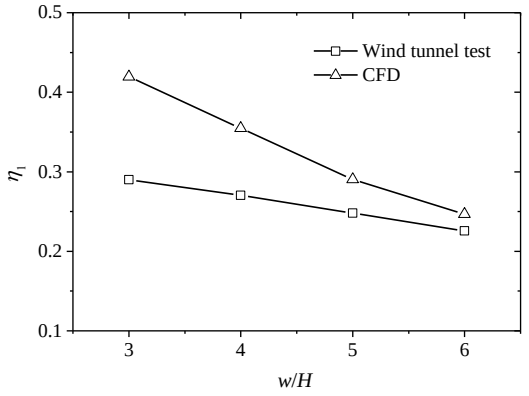

(a) η_1

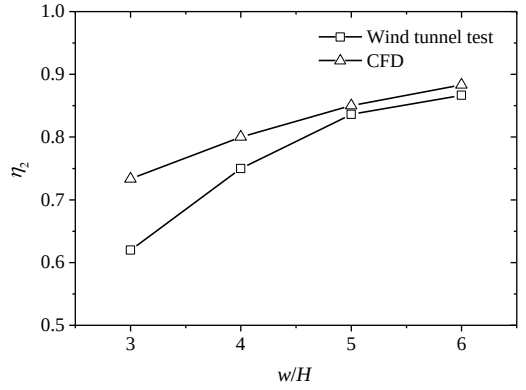

(b) η_2

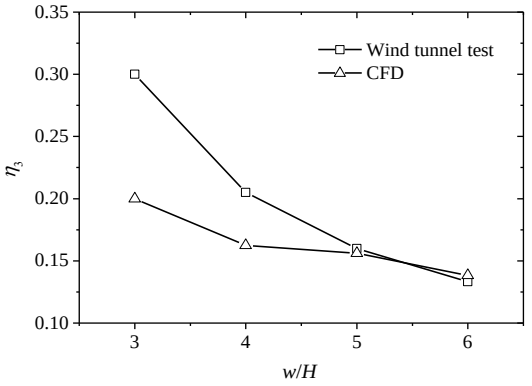

(c) η_3

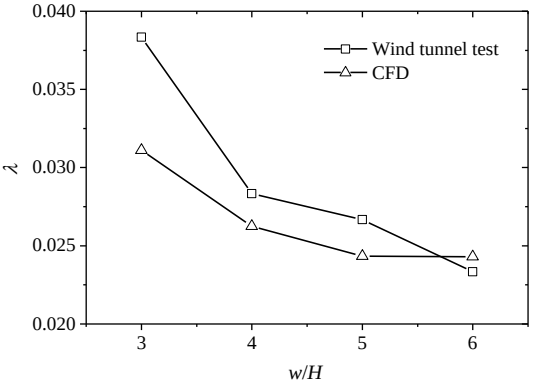

(d) λ

Fig. 19 The characteristic of snow distribution on lower roofs

When the width-height ratio increases, the effect of flow around the model on the centerline section (y/H=0) begins to weaken and the friction velocity decreases (Fig. 17) which results in less erosion of snow. Thus, the η_1 of frontal region at the centerline section (y/H=0) is shorter than the model with smaller width-height ratio. The dimensionless length η_2 is gradually getting to increase with the increase of width-height ratio (Fig. 19(b)), which indicates that the erosion of rear region is less for the larger width-height ratio. However, the η_1 and η_2 in the numerical simulation is larger than that in the wind tunnel test, and especially the difference is more significant for the model that has a relatively small width-height ratio ($w/H \le 4.0$). The dimensionless length η_3 and dimensionless area λ both decrease as the width-height ratio increases, while the results in the numerical simulation is smaller than that in the wind tunnel test.

The relative area of exposed roof caused by severe erosion is smaller at the condition of larger width-height ratio, which means the distribution of snow at the transverse dimension at the rear region gets more uniform. As one can see from Fig. 19, the erosion amount in the numerical simulation is smaller than that in the wind tunnel test in general. Although there exist some differences between the results calculated by CFD simulations and the results obtained from wind tunnel tests, the overall trend is consistent. Therefore, the results obtained by numerical simulations based on adaptive-mesh method with RBF interpolation are acceptable.

5.3 Mass transport rate

Fig. 20 compares the volume of total erosion of snow particles or silica sand on lower roofs between the numerical simulation and wind tunnel test, where the volume of total erosion is equal to $\iint \Delta h(x,y)dxdy$ in Eq. (7). Both the numerical simulations and wind tunnel tests show the total erosion linearly increases as the width-height ratio increases. The total erosion obtained by the numerical simulation accords with the wind tunnel test results, which means that the numerical simulation method used in this paper can effectively predict the snow drifting on stepped flat roofs.

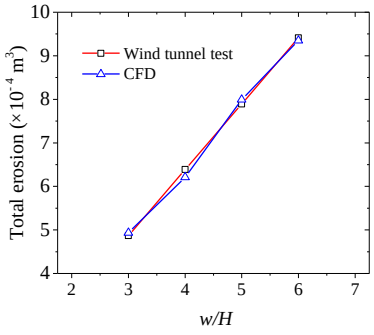

Fig. 20 Total erosion for the numerical simulation and wind tunnel test

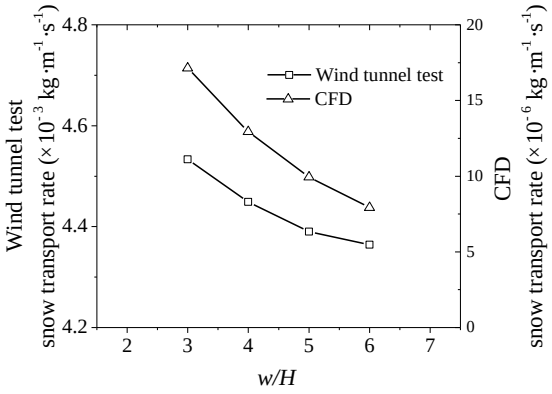

Fig. 21 Mean mass transport rate Q_m for the numerical simulation and wind tunnel test

Fig. 21 shows the mean transport rate obtained from both the numerical simulation and wind tunnel test using Eq. (7). Although the order of magnitude of the mean mass transport rate is different between the wind tunnel test and the numerical simulation, the overall trend of both is consistent which nonlinearly decreases as the width-height ratio increases. The mean mass transport rate is mainly affected by flow fields. Combined with Figs. 17 and 18, the different building geometry has a different flow field so that the mean mass transport rate is different.

To further analyze the effect of width-height ratio on the mass transport rate during the process of snow drifting, the relationship between the average mass transport rate and stage n is shown in Fig. 22. The mean mass transport rate gradually decreases for a single model and is getting to be stable with the development of calculation stage. For example, the mean transport rate at Stage 1_E is 2.47×10^{-5} kg·m^{-1}·s^{-1} and it is 1.76×10^{-5} kg·m^{-1}·s^{-1}, 1.39×10^{-5} kg·m^{-1}·s^{-1} and 1.24×10^{-5} kg·m^{-1}·s^{-1} for Stage 2_E to 4_E, respectively. The mean mass transport rate of w/H=3.0 is significantly higher than others at each stage and it is a direct explanation why the overall erosion of the model with a relatively small width-height ratio is larger.

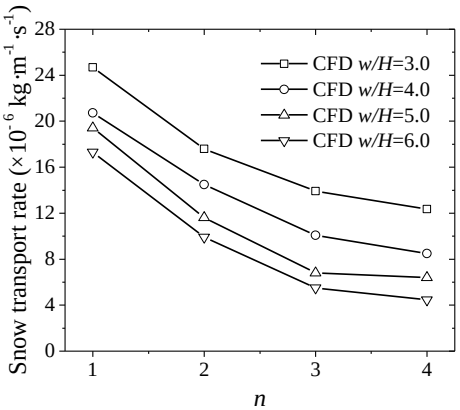

Fig. 22 Mean mass transport rate Q_m for each stage

6. Conclusions

Scale stepped flat roof tests are conducted in wind tunnel to analyze the effect of width-height ratio on the snow drifting on lower roofs, in which silica sand is used to model the snow particle. An adaptive-mesh method using RBF interpolation for stepped flat roofs is used to simulate the dynamic process of snow cover boundary and then a time-marching analysis of steady snow drifting on stepped flat roofs, which has the same width-height ratio with the wind tunnel test, is conducted in detail. The comparison between the results from the numerical simulation and wind tunnel test validates the accuracy of the numerical method to a certain degree. Some conclusions can be drawn from the present study as follows:

(1) The snow erosion mainly concentrate on the front and rear region on the lower roof, while the deposition of snow occurs at the middle region with small quantity. As the width-height ratio w/H increases, the erosion of snow at the front and rear region decreases on the centerline section (y/H=0) and the percentage of erosion on lower roofs decreases systematically as well. With the increase of the width-height ratio w/H, the relative area of exposed roofs at the rear region decreases, therefore the distribution of snow depth looks like more uniform in the transverse direction on lower roofs.

(2) The friction velocity u_* gradually decreases at the front region and increases at the rear region from Stage 1_S to Stage 4_S for a certain model and the mean friction velocity u_{*m} decreases with the increase of width-height ratio.

(3) The volume of total erosion linearly increases as width-height ratio increases, however, the mean mass transport rate of snow particles or silica sand nonlinearly decreases with the increase of width-height ratio. The mass transport rate is significantly high in the process of snow drifting when the model has a relatively small width-height ratio, which directly results in large erosion of snow on lower roofs.

(4) The adaptive-mesh method based on RBF interpolation is used to simulate the dynamic process of snow boundary on the stepped flat roof in this paper, and then a time-marching analysis of steady snow drifting on lower roofs is conducted. In general, the characteristic of snow distribution on lower roofs obtained from the numerical simulation is basically similar to the wind tunnel test results. The snow distribution on the centerline section (y/H=0) from both the numerical simulation and wind tunnel test are compared with field observations, and the overall trend is generally consistent. The numerical simulation basically reproduces the phenomenon which occurs in the wind tunnel test.

In the present study, the wind velocity and the incidence angle of wind are kept the same in the wind tunnel test and numerical simulation. However, the different wind velocity and directions will affect the snow distribution on roofs in nature. In the future, the different wind velocity and the incidence angle of wind will be considered to further study the relationship between them and snow distribution on roofs.

Acknowledgments

This project is supported by National Key R&D Plan (grant number 2016YFC0802205-1) and National Natural Science Foundation of China (grant number 51378428).

References

Anno, Y. (1984), "Requirements for modeling of a snowdrift", *Cold Reg. Sci. Technol*., **8**(3), 241-252.

Anno, Y. (1985), "Modelling a snowdrift by means of activated clay particles", *Ann. Glaciol*., **6**(1), 48-52.

ANSYS Fluent User's Guide 16.1

Beyers, J.H.M., Sundsbø, P.A. and Harms, T.M. (2004), "Numerical simulation of three-dimensional, transient snow drifting around a cube", *J. Wind Eng. Ind. Aerod*., **92**(9), 725-747.

Beyers, M. and Waechter, B. (2008), "Modeling transient snowdrift development around complex three-dimensional structures", *J. Wind Eng. Ind. Aerod*., **96**(10), 1603-1615.

Bintanja, R. (2000), "Snowdrift suspension and atmospheric turbulence, Part I: Theoretical background and model description", *Bound.-Lay. Meteorol*., **95**(3), 343-368.

Blocken, B. (2015), "Computational fluid dynamics for urban physics: Importance, scales, possibilities, limitations and ten tips and tricks towards accurate and reliable simulations", *Build. Environ*., **91**, 219-245.

Dvorak, F.A. (1969), "Calculation of turbulent boundary layers on rough surfaces in pressure gradient", *AIAA J*., **7**(9), 1752-1759.

Franke, J., Hellsten, A., Schlünzen, H. and Carissimo, B. (2007), "Best practice guideline for the CFD Simulation of Flows in the Urban Environment", COST Office, Brussels. (3-00-018312-4).

Haehnel, R.B., Wilkinson, J.H. and Lever, J.H. (1993), "Snowdrift modeling in the CRREL wind tunnel", *Proceedings of the 50th Eastern Snow Conference*, Quebec City, Quebec, June, 8-10.

Humphrey, J.A.C. (1990), "Fundamentals of fluid motion in erosion by solid particle impact", *Int. J. Heat Fluid. Fl*., **11**(3), 170-195.

Isyumov, N. and Mikitiuk, M. (1990), "Wind tunnel model tests of snow drifting on a two-level flat roof", *J. Wind Eng. Ind. Aerod*., **36**, 893-904.

Isyumov, N. and Mikitiuk, M. (1992), "Wind tunnel modeling of snow accumulations on large-area roofs", *Proceedings of the second International Conference on Snow Engineering*, 181-193.

Iversen, J.D. (1979), "Drifting snow similitude-drift deposition rate correlation", *Proceedings of the 5th International Conference on Wind Engineering. Pergamon Press*, Fort Collins, 1037-1080.

Iversen, J.D. (1980), "Drifting-snow similitude—transport-rate and roughness modeling", *J. Glaciol*., **26**(94), 393-403.

Kind, R.J. (1976), "A critical examination of the requirements for model simulation of wind-induced erosion/deposition phenomena such as snow drifting", *Atmos. Environ*., **10**(3), 219-227.

Kind, R.J. (1986), "Snowdrifting: a review of modelling methods", *Cold Reg. Sci. Technol*., **12**(3), 217-228.

Kind, R.J. and Murray, S.B. (1982), "Saltation flow measurements relating to modeling of snowdrifting", *J. Wind Eng. Ind. Aerod*., **10**(1), 89-102.

Kuroiwa, D., Mizuno, Y. and Takeuchi, M. (1967), "Micromeritical properties of snow", *Proceedings of the*

International Conference on Low Temperature Science: Physics of Snow and Ice, **1**, 751-772 (2).

Kwok, K.C.S., Kim, D.H., Smedley, D.J. and Rohde, H.F. (1992), "Snowdrift around buildings for Antarctic environment", *J. Wind Eng. Ind. Aerod*., **44**(1-3), 2797-2808.

Liston, G.E., Brown, R.L. and Dent, J. (1994), "A computational model of two phase, turbulent atmospheric boundary layer with blowing snow", *Proceedings of the Workshop on the Modelling of Windblown Snow and Sand*.

Liston, G.E., Brown, R.L. and Dent, J.D. (1993), "A two-dimensional computational model of turbulent atmospheric surface flows with drifting snow", *Ann. Glaciol*., **18**(1), 281-286.

Liston, G.E. and Sturm, M. (1998), "A snow-transport model for complex terrain", *J. Glaciol*., **44**(148), 498-516.

Liu, M., Zhang, Q., Fan, F. and Shen, S. (2018), "Experiments on natural snow distribution around simplified building models based on open air snow-wind combined experimental facility", *J. Wind Eng. Ind. Aerod.*, **173**, 1-13.

Majowiecki, M. (1998). "Snow and wind experimental analysis in the design of long-span sub-horizontal structures", *J. Wind Eng. Ind. Aerod*., **74**, 795-807.

Murakami, S. (1993), "Comparison of various turbulence models applied to a bluff body", *J. Wind Eng. Ind. Aerod*., **46**, 21-36.

Murakami, S., Mochida, A. and Kato, S. (2003), "Development of local area wind prediction system for selecting suitable site for windmill", *J. Wind Eng. Ind. Aerod*., **91**(12), 1759-1776.

Naaim, M., Naaim-Bouvet, F. and Martinez, H. (1998), "Numerical simulation of drifting snow: erosion and deposition models", *Ann. Glaciol*., **26**, 191-196.

O'Rourke, M., DeGaetano, A. and Tokarczyk, J.D. (2004), "Snow drifting transport rates from water flume simulation", *J. Wind Eng. Ind. Aerod*., **92**(14), 1245-1264.

Okaze, T., Takano, Y., Mochida, A. and Tominaga, Y. (2015), "Development of a new k–ε model to reproduce the aerodynamic effects of snow particles on a flow field", *J. Wind Eng. Ind. Aerod*., **144**, 118-124.

Powell, M.J. (1987), "Radial basis functions for multivariable interpolation: a review", *Proceeding of the Algorithms for approximation*, Clarendon Press, 143-167.

Sato, T., Uematsu, T., Nakata, T. and Kaneda, Y. (1993), "Three dimensional numerical simulation of snowdrift", *J. Wind Eng. Ind. Aerod*., **46**, 741-746.

Satoh, K. and Takahashi, S. (2006), "Threshold wind velocity for snow drifting as a function of terminal fall velocity of snow particles", *Bull. Glaciol. Res*., **23**(26), 13-21.

Schaelin, A., Ilg, L. and Benesch, M. (2004), "Sow deposition around mountain hut-design optimization by CFD and scaled water channel model and realization of solutions", *Proceedings of the Fifth International Conference on Snow Engineering*, 5-8 July, Davos, Switzerland (p. 147), CRC Press.

Serine, A., Shimura, M., Maruoka, A. and Hirano, H. (1999), "The numerical simulation of snowdrift around a building", *Int. J. Comput. Fluid. D*., **12**(3-4), 249-255.

Smedley, D.J., Kwok, K.C.S. and Kim, D.H. (1993), "Snowdrifting simulation around davis station workshop, Antarctica", *J. Wind Eng. Ind. Aerod*., **50**, 153-162.

Sundsbø, P.A. (1998), "Numerical simulations of wind deflection fins to control snow accumulation in building steps", *J. Wind Eng. Ind. Aerod*., **74**, 543-552.

Tominaga, Y. (2017), "Computational fluid dynamics simulation of snowdrift around buildings: Past achievements and future perspectives", *Cold. Reg. Sci. Technol*., **150**, 2-14.

Tominaga, Y., Akabayashi, S.I., Kitahara, T. and Arinami, Y. (2015), "Air flow around isolated gable-roof buildings with different roof pitches: Wind tunnel experiments and CFD simulations", *Build. Environ*., **84**, 204-213.

Tominaga, Y., Mochida, A., Yoshie, R., Kataoka, H., Nozu, T., Yoshikawa, M. and Shirasawa, T. (2008), "AIJ guidelines for practical applications of CFD to pedestrian wind environment around buildings", *J. Wind Eng. Ind. Aerod*., **96**(10), 1749-1761.

Tominaga, Y., Mochida, A., Yoshino, H., Shida, T. and Okaze, T. (2006), "CFD prediction of snowdrift around a cubic building model", *Proceeding of the fourth International Symposium on Computational Wind Engineering (CWE2006)*, Yokohama, Japan Vol. 26.

Tominaga, Y., Okaze, T. and Mochida, A. (2011), "CFD modeling of snowdrift around a building: An overview of models and evaluation of a new approach", *Build. Environ*., **46**(4), 899-910.

Tominaga, Y., Okaze, T., Mochida, A., Nemoto, M. and Ito, Y. (2009), "Prediction of snowdrift around a cube using CFD Model incorporating effect of snow particles on turbulent flow", *Proceeding of the seventh Asia-Pacific Conference on Wind Engineering*, Taipei, Taiwan.

Tsuchiya, M., Tomabechi, T., Hongo, T. and Ueda, H. (2002), "Wind effects on snowdrift on stepped flat roofs", *J. Wind Eng. Ind. Aerod*., **90**(12-15), 1881-1892.

Tutsumi, T., Chiba, T. and Tomabechi, T. (2012), "Snowdrifts on and around buildings based on field measurement", *Proceedings of the 7th International Conference on Snow Engineering (Snow Engineering VII)*, Fukui, Japan.

Uematsu, T., Nakata, T., Takeuchi, K., Arisawa, Y. and Kaneda, Y. (1991), "Three-dimensional numerical simulation of snowdrift", *Cold Reg. Sci. Technol*., **20**(1), 65-73.

Wang, W.H., Liao, H.L. and Li, M.S. (2013), "Numerical simulation of wind-induced roof snow distributions based on time variable boundary", *J. Southwest Jiaotong Univ*., **5**, 851-856+967 (in Chinese).

Wang, W.H., Liao, H.L. and Li, M.S. (2014), "Wind tunnel test on wind-induced roof snow distribution", *Build. Struct*., **35**(5), 135-141. (in Chinese).

Zhao, L., Yu, Z., Zhu, F., Qi, X. and Zhao, S. (2016). "CFD-DEM modeling of snowdrifts on stepped flat roofs", *Wind Struct*., **23**(6), 523-542.

Zhou, X., Hu, J. and Gu, M. (2014), "Wind tunnel test of snow loads on a stepped flat roof using different granular materials", *Nat. Hazards*, **74**(3), 1629-1648.

Zhou, X., Kang, L., Gu, M., Qiu, L. and Hu, J. (2016), "Numerical simulation and wind tunnel test for redistribution of snow on a flat roof", *J. Wind Eng. Ind. Aerod*., **153**, 92-105.

Zhou, X., Kang, L., Yuan, X. and Gu, M. (2016), "Wind tunnel test of snow redistribution on flat roofs", *Cold Reg. Sci. Technol*., **127**, 49-56.

Zhu, F., Yu, Z., Zhao, L., Xue, M. and Zhao, S. (2017), "Adaptive-mesh method using RBF interpolation: A time-marching analysis of steady snow drifting on stepped flat roofs", *J. Wind Eng. Ind. Aerod*., **171**, 1-11.

CC